Research Article

Superlubricity of epitaxial monolayer WS$_2$ on graphene

Holger Büch[1], Antonio Rossi[1,2], Stiven Forti[1], Domenica Convertino[1,2], Valentina Tozzini[2], and Camilla Coletti[1,3] (✉)

[1] *Center for Nanotechnology Innovation @NEST, Istituto Italiano di Tecnologia, Piazza S. Silvestro 12, 56127 Pisa, Italy*

[2] *NEST, Istituto Nanoscienze – CNR and Scuola Normale Superiore, Piazza San Silvestro 12, 56127 Pisa, Italy*

[3] *Graphene Labs, Istituto Italiano di Tecnologia, Via Morego 30, 16163 Genova, Italy*

ABSTRACT

We report the superlubric sliding of monolayer tungsten disulfide (WS$_2$) on epitaxial graphene (EG) grown on silicon carbide (SiC). Single-crystalline WS$_2$ flakes with lateral size of hundreds of nanometers are obtained via chemical vapor deposition (CVD) on EG. Microscopic and diffraction analyses indicate that the WS$_2$/EG stack is predominantly aligned with zero azimuthal rotation. The present experiments show that, when perturbed by a scanning probe microscopy (SPM) tip, the WS$_2$ flakes are prone to slide over the graphene surfaces at room temperature. Atomistic force field-based molecular dynamics simulations indicate that, through local physical deformation of the WS$_2$ flake, the scanning tip releases enough energy to the flake to overcome the motion activation barrier and trigger an ultralow-friction rototranslational displacement, that is superlubric. Experimental observations show that, after sliding, the WS$_2$ flakes come to rest with a rotation of $n\pi/3$ with respect to graphene. Moreover, atomically resolved measurements show that the interface is atomically sharp and the WS$_2$ lattice is strain-free. These results help to shed light on nano-tribological phenomena in van der Waals (vdW) heterostacks, and suggest that the applicative potential of the WS$_2$/graphene heterostructure can be extended by novel mechanical prospects.

1 Introduction

Owing to their attractive electronic, optical, and magnetic properties, two-dimensional (2D) van der Waals (vdW) heterostacks serve as a platform for fundamental studies and display a wide range of potential applications [1, 2]. Among the broad range of possible 2D heterostacks, those obtained by combining transition metal dichalcogenides (TMDs) and graphene currently attract considerable interest, owing to their appealing optoelectronic properties. In particular, tungsten disulfide (WS$_2$) TMD exhibits large carrier mobility [3], high photoluminescence emission [4], significantly large spin-orbit splitting (~ 460 meV) [5],

Address correspondence to camilla.coletti@iit.it

as well as long exciton life and coherence times [6]. Novel field-effect vertical tunneling transistors [7] and photodetectors [8, 9] based on WS_2/graphene stacks have been demonstrated. Although the optoelectronic potential of this 2D heterostack is being extensively studied, relatively little attention has been paid to its nanotribological properties. Both graphite and bulk WS_2 are known as effective lamellar lubricants with hexagonal structures. In the past years, a number of tribological experiments have been carried out on both graphite and bulk molybdenum disulfide (MoS_2), whose structure is analogous to that of WS_2, and novel interesting phenomena such as self-retraction and superlubricity have been reported [10–13].

The term superlubricity, indicating a vanishing friction, was first introduced in the early 1990s by Hirano et al. [14–16], who related the friction to the lack of "commensuration" between crystal surfaces. This was in turn defined in terms of the difference between lattice parameters, symmetry, and relative rotation of the surfaces [14]. Parameters related to the commensuration were introduced in subsequent studies, such as the "registry index" [17], measuring the rigid geometrical superposition of atoms at the (possibly rotated) surfaces. However, it was later recognized [18] that the relaxation of the atoms at the surface has a fundamental role, i.e., it introduces an energy dissipation mechanism. The dissipation was linked to the flexibility of the surfaces [18] by the parameter $\lambda = u/(Ka^2)$, measuring the relative strength of the inter-surface interaction u (usually the vdW interaction) and the rigidity of the surfaces K, with a being the lattice parameter. A system would be prone to superlubricity if the surfaces in contact are rather rigid (large K) and/or the inter-surface interaction u is weak. In fact, the effect of vertical flexibility and relaxation of the surfaces was shown to reduce the role of the commensurability in the lubricity phenomenon [19], while at the same time enhancing the impact of flexural phonons. The phenomenon of superlubricity displays several nontrivial aspects, and no broad consensus has been reached yet, even on the definition of the term itself. In this work, the term superlubricity is used to describe a 2D flake sliding over a substrate without requiring a horizontal force, in a non-diffusive regime.

According to this definition, superlubricity was previously observed for a graphene flake attached to an atomic force microscopy (AFM) tip, sliding over a graphite substrate [20]. The phenomenon was also reported in scanning tunneling microscopy (STM) experiments at temperatures as low as 5 K [21]. Very recently, friction tests on the sliding motion of a single-layer MoS_2 nanoflake on another incommensurate and misaligned MoS_2 substrate yielded ultralow friction coefficients of about 10^{-4}, indicating superlubricity [22]. Similarly, extremely low friction values were measured upon sliding a multilayer graphene-coated microsphere on graphite and bulk hexagonal boron nitride (hBN) [23]. In addition, rotation and translation of graphene flakes on hBN via AFM–tip interactions have been previously reported [24]. A number of theoretical studies have predicted superlubricity in vertical homo- and heterostacks of 2D materials [25, 26]. However, superlubricity between a TMD and graphene (a natural platform for nanotribological studies) has not been experimentally observed to date.

Herein, we report the superlubric sliding of monolayer WS_2 nanoflakes over single-layer epitaxial graphene (EG), triggered by an STM tip. WS_2 was synthesized on EG grown on silicon carbide (SiC) via chemical vapor deposition (CVD) [27]. Compared to heterostacks obtained via mechanical exfoliation, this entirely bottom-up heterostack presents a WS_2/graphene interface free of resist and solution residuals, and it is thus ideal for nanotribology investigations. The experimental results were analyzed using classical molecular dynamics simulations, which show that the simple interaction of a WS_2 flake with a scanning tip is sufficient to trigger its sliding.

2 Materials and methods

Graphene was obtained via solid-state thermal decomposition of atomically flat, nominally on-axis 6H–SiC(0001) using a resistively-heated cold-wall reactor [28]. The as-grown graphene/SiC samples were then used as receiving substrates in a tube furnace low-pressure CVD reactor, while sulfur and tungsten trioxide powders served as chemical precursors and argon was used as carrier gas [27]. STM measurements were carried out in an Omicron

low-temperature STM system. After transfer to an ultrahigh vacuum (UHV) chamber, the sample was annealed via resistive heating to 400 °C for about 12 h. The scanning tunneling microscope was operated in constant current mode using an etched tungsten tip. The tip voltage and tunnel current were varied in the 0.1–2.7 V and 10–300 pA ranges, respectively. The pressure in the STM chamber was better than 5×10^{-11} mbar. Scanning electron microscopy (SEM) images were recorded at 5 keV using a Zeiss Merlin microscope equipped with a field emission gun. AFM measurements were performed using an AFM+ instrument by Anasys. The Gwyddion software package was used for the analysis of the STM and AFM images [29]. The AFM videos included in the Electronic Supplementary Material (ESM) were generated from subsequent AFM scans. Low-energy electron diffraction (LEED) measurements were carried out with a SPECS ErLEED system. All measurements were performed at room temperature (RT).

Molecular dynamics simulations were performed with a model system including a rhombohedral graphene sheet of ~ 32 nm lateral size and triangular WS_2 flakes of ~ 5, 10, or 20 nm side. In order to speed up the simulations, a minimalist connective model, the elastic network, was used to represent the internal dynamics of both graphene sheet and flake. The interaction parameters were optimized to reproduce experimental measurements or data derived from higher order models. The flake-substrate interactions were represented via a Lennard–Jones (LJ) potential with standard parameterization. A preliminary evaluation of the vdW energy, performed by a geometry optimization on the flat substrate, yielded a vdW energy of about 110 meV·atom^{-1}. This value is of the same order, although larger, than that obtained by density functional theory (DFT) calculations in our previous work [5]. This discrepancy might be due to different causes (registry and corrugation, underestimation of vdW energy in DFT); therefore, since a direct estimate of the experimental value of this parameter is not available, we used the standard values of the vdW parameters, which have been widely used and tested. The whole parameter set, as well as additional details on the model systems and force field, are reported in the ESM. The simulations

were performed with the DL_POLY code [30], using software tools developed in-house to create the input files and analyze the results. The simulation timestep was set to 1 fs and standard algorithms (Verlet, with a Nosé thermostat for constant temperature runs) were used for integrating the equations of motion. The simulations were performed on an eight-core workstation.

3   Results and discussion

3.1   WS$_2$ sliding triggered by a scanning probe microscopy (SPM) tip

Figure 1(a) shows a large-scale filled-state STM image of as-grown triangular WS$_2$ flakes on the graphene/SiC substrate.

A few WS$_2$ flakes are visible within the field of view, with an apparent height of ~ 7 Å (see line profile in the inset of Fig. 1(a)), confirming the monolayer thickness of the TMD. Most flakes lie smoothly across the SiC step edges (~ 8 Å in height) and their size distribution is appreciably narrow. The average side length of the flakes analyzed in the sample is
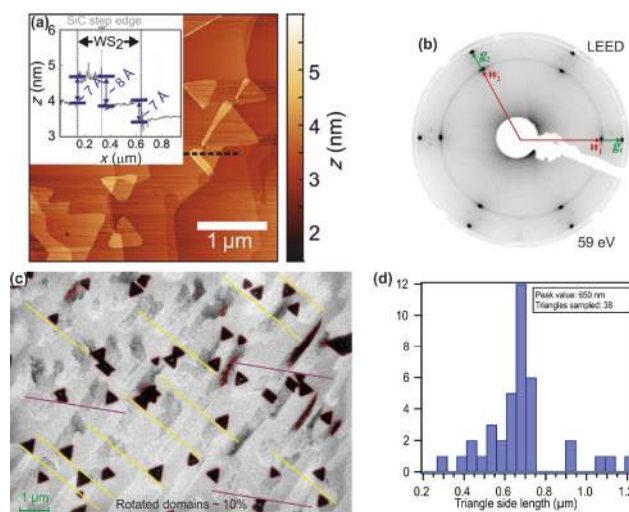

Figure 1   (a) Large-scale STM image of WS$_2$ flakes on the graphene/SiC(0001) substrate, recorded at a tip voltage 2.7 V and a constant current of 0.3 nA. The black dashed line marks the position of the line profile displayed in the inset. (b) LEED pattern of the WS$_2$/graphene/SiC heterostructure recorded at a primary beam energy of 72 eV. The arrows mark the different diffraction spots. (c) Representative SEM micrograph highlighting the main orientations of the WS$_2$ crystals. (d) Histogram of the grain side length obtained from the analysis of the SEM image in (c).

about 600 nm, corresponding to an area of about 0.16 μm^2, as confirmed by SEM analysis (see the histogram in Fig. 1(d)). Larger areas shown in the histogram typically result from the merging of triangular grains (i.e., the detected values are multiples of those obtained for isolated crystals). A simple inspection of the STM and SEM micrographs reveals an epitaxial relationship with the substrate. In fact, the majority of the triangular flakes exhibit parallel edges. As shown in Fig. 1(c), only a limited number of flakes (~ 10%) exhibited edges rotated by 30°. The LEED analysis shown in Fig. 1(b), performed on a macroscopic area of about 1 mm^2, reveals that the majority of the WS_2 flakes are perfectly aligned with the substrate, as the highest-intensity WS_2 diffraction spots are oriented at 0° with respect to the graphene diffraction spots. We also note a faint complete circle in the LEED image, corresponding to reciprocal lattice vectors of WS_2, which we attribute to a low percentage of WS_2 nanoflakes of stray orientation. Our result differ from those reported by Miwa et al. [31] for MoS_2/graphene heterostacks synthesized in vacuum, where the TMD was found to be rotated by 30° with respect to the graphene Brillouin zone (BZ). On the other side, a similar distribution of flake orientations was previously observed for CVD-grown TMD/graphene [5, 32], which suggests that the vapor-phase approach is a suitable technique to obtain heterostructures with azimuthal alignment.

Figures 2(a)–2(c) illustrate the typical behavior observed upon scanning with an STM tip over sample regions containing WS_2 flakes.

The figures show three subsequent STM scans of the same surface region, displaying a WS_2 flake in three different positions (marked by arrows). Initially, the WS_2 flake is located in the bottom-right portion of the image (Fig. 2(a)). In the subsequent image, the flake has moved to the center-left area of the micrograph (Fig. 2(b)), and finally, in the third scan, it is found in the bottom left side (Fig. 2(c)). Hence, it appears that, upon triggering by the STM tip, the flake slides over the substrate by rotating and translating in random directions, not related with the scanning direction. It should be mentioned that the sliding of the WS_2 flake on top of the graphene substrate is not always observed in STM imaging
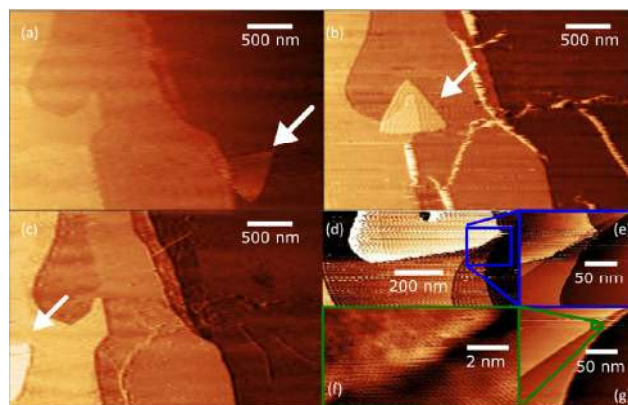
Figure 2 (a)–(c) STM images of the same area, displaying three different positions of a WS_2 flake (marked by arrows) in subsequent scans. Tip parameters: voltage of +2.7 V and constant tunneling current of 0.3 nA. (d) STM image (2.5 V, 0.1 nA) of a surface region containing a WS_2 flake (partially seen in a brighter color on the top end). (e) Enlarged view of the area marked by a box in (d). (g) Subsequent STM scan showing that the WS_2 flake is no longer visible. (f) Enlarged view of the area marked in (g), revealing intact graphene at the position previously occupied by the WS_2 flake.

experiments. The scanned WS_2 flake might either sit still or move suddenly to another position, often located several micrometers away (i.e., outside the field of view of the scan), according to what appears to be a stochastic trigger (i.e., the sliding of the flake becomes more likely the longer we scan over it). Figure S1 in the ESM shows the behavior typically observed for larger scan areas, where some of the flakes sit still while others slide around without a preferential direction. The locked flakes are often part of large clusters of flakes or sit across step edges. After each transition the WS_2 flakes are always found in a position commensurate with the underlying graphene layer. They either maintain the same initial orientation or rotate by 60°, reasonably indicating the most stable stacking.

We should point out that the present observation of a sudden and fast sliding motion of a WS_2 flake over a graphene substrate is in contrast with previous experimental findings for similar systems, such as MoS_2 on epitaxial graphene and MoS_2 on graphite [32–34]. However, WS_2 on epitaxial graphene has already been reported to differ from related systems in several aspects, all of which point to a weaker interaction of WS_2 with epitaxial graphene on SiC, compared with MoS_2 [5, 35].

Our experiments did not show a specific trend in the moving probability as a function of the tip voltage (while keeping the tip-sample distance constant). This observation rules out electrostatic effects as the triggering factor of the sliding motion, as was reported in electrostatic manipulation STM (EM-STM) experiments [36, 37]. This is further confirmed by the observation of non-directional WS_2 sliding triggered by an AFM probe. When scanning in contact mode, some of the WS_2 flakes rotate and translate, as shown in Fig. S2 and in Videos ESM3 and ESM4 in the ESM, in agreement with the STM measurements. In contrast, no WS_2 flake movement is observed in tapping mode, which we attribute to the much shorter time during which the vdW forces between tip and sample reach full strength. Since both sample and probe are grounded during the AFM scan, electrostatic manipulation does not represent the driving force of the observed sliding. Moreover, these observations are significantly different from those reported in a previous study by Kobayashi et al., in which WS_2 grains were manipulated and physically pushed with a nanoprober system [38].

The detailed analysis of STM and subsequent AFM scans indicates that the sliding flakes typically come to rest at the edge of steps (or when approaching flake clusters), until they are triggered again by the tip (see the ESM). Hence, typical sliding distances for the WS_2 flakes range from 500 nm to a few micrometers (corresponding to the terrace widths for the samples analyzed). In addition, we note that the flakes can climb steps both upward and downward. Statistically, we find that climbing up is more likely on steps of lower heights (i.e., on bilayer slabs of SiC rather than unit cell-high steps, see the ESM).

The sliding of the WS_2 flakes does not induce defects in the underlying graphene, as shown in Figs. 2 (d)–2(g). Figure 2(d) shows a larger-area scan, to clearly display the initial presence of the WS_2 flake, whereas Fig. 2(e) shows an enlarged view of one of its edges. In the micrograph shown in Fig. 2(g), obtained immediately after that displayed in Fig. 2(e), the flake appears to have slid away. The corresponding enlarged view (Fig. 2(f)) shows that the graphene layer located in the position previously occupied by the WS_2 flake retains its lattice structure, with no alteration

of atomic registry. The sliding behavior observed in this work appears very similar to that reported in reference [21], where superlubric sliding of graphene flakes on graphite was triggered by an STM tip. To further clarify the triggering mechanism for the specific system investigated in this study, molecular dynamics simulations were carried out and are discussed in the following section.

3.2 Molecular dynamics simulations

Before investigating the tip-triggered motion, we performed simulations aimed at investigating whether the motion of the WS_2 flakes on graphene can be thermally activated. We performed simulations at different temperatures and involving different flake sizes (see the ESM for a detailed list of the simulations carried out). For all flake sizes, we observe an oscillating horizontal motion of the flake at low temperatures, while the translational motion becomes activated at higher temperatures. In some cases, the latter motion is preceded by an oscillating percolation phase, in which we also observe two preferential orientations, namely 0° or 30° and their equivalents (see Figs. 3(a) and 3(c), displaying a flake of ~ 10 nm side at ~ 200 K, and the plots and videos in the ESM).

The activation temperature of the translational motion (T_c) depends on the size: We observe a clear dependence on the square root of the number of atoms (or flake area), or, equivalently, a linear dependence on the side of the flake (see the data points plotted in Fig. 3(b)). Therefore, the translational motion is thermally activated for flakes with lateral size of a few tens of nanometers even at room temperature, while larger flakes appear steady. Interestingly, the duration of the oscillatory phase depends on the temperature and flake size.

This result can be explained within the framework of the general phase transition theory. In general, a transition occurs when $k_B T$ overcomes a given energy barrier ΔE. This value, in the case of thermal activation, is related to the static friction coefficient, and approximately corresponds to the flake-substrate interaction per unit surface. A rough estimate can be obtained from the average vdW energy per contact atom ε: The simulations return values between –108 and –112 meV, also depending on the temperature
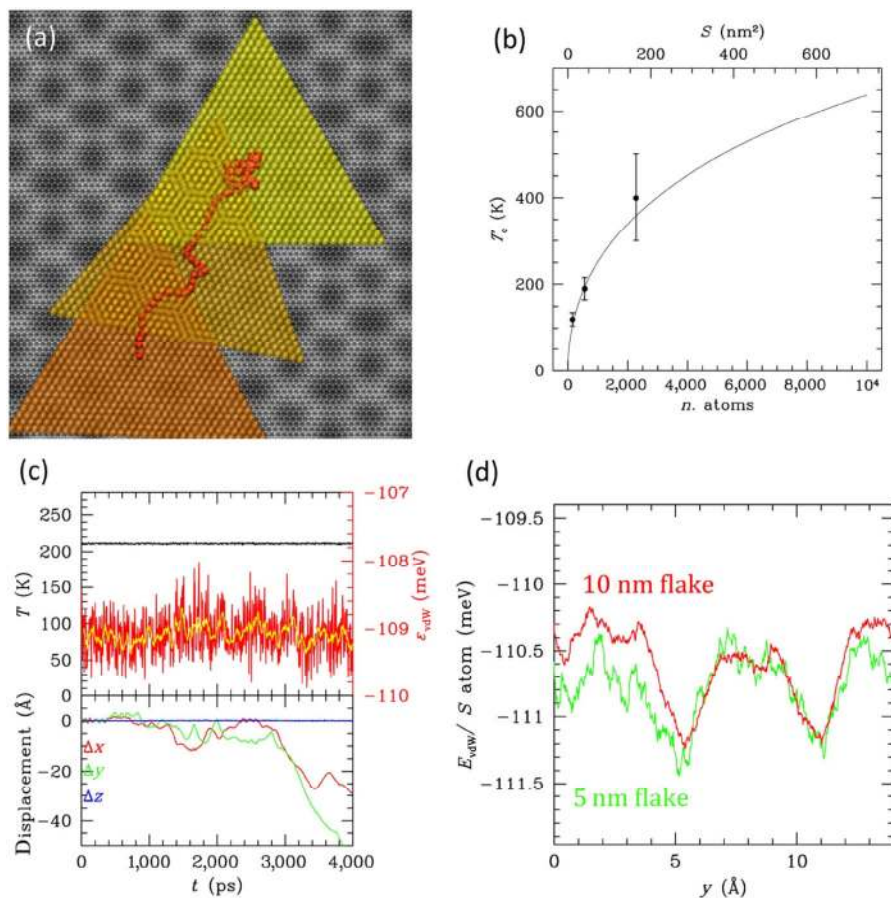
Figure 3 (a) Thermal activation of the motion of a flake of ~ 10 nm at ~ 200 K on graphene (the corrugation of the substrate is highlighted). Red dots represent the trajectory of the center of the flake, which also undergoes a rotational motion, as shown by selected configurations displayed in the figure (yellow = first, dark orange = last). (b) Transition temperatures as a function of the flake size, as deduced by simulations. The line is a fit to the interpolation relationship $T_c = T_\infty/(1+\sqrt{S_0/S})$, where T_∞ is the transition temperature in the thermodynamic limit and S_0 a parameter representing the critical size for the crossover to the thermodynamic limit; the number of mobile flakes with respect to the total number of flakes at a given temperature and size will then be $\rho = \exp(-T/T_c)$. (c) Temperature, vdW energy, and displacement (in the three Cartesian directions) corresponding to the simulation of (a). The oscillatory phase is clearly visible up to 3 ns, with a preliminary phase with very small oscillations up to 0.5 ns, subsequently increasing in amplitude up to the start of the translational motion. The displacement in the z direction is always near to zero. (d) Energy profile corresponding to sliding process of flakes of 5 and 10 nm subject to a constant force in the y (armchair) direction and to overdamping (see the ESM for details).

(see Fig. 3(c)), pointing to an activation temperatures exceeding 1,000 K. However, this simplified picture assumes the thermodynamic limit, i.e., very large flakes. In the case of small flakes, the transition is driven by the amplitude and correlation length of the energy fluctuations (diverging near T_c), rather than by the average value of the energy. Because fluctuations scale as the square root of the number of particles, this explains the observed behavior. The transition temperature as a function of the size fitted according to this rationale on simulation data is reported in Fig. 3(b). In fact, according to our simulation data,

flake with lateral size of 20–50 nm are expected to be mobile at RT, whereas flakes of 100 nm side have thermal activation temperatures above RT. The thermal activation of nanometer-size flakes at RT might explain well the absence of such flakes in our experimental analysis.

Hence, for the flakes studied in the present experiments, with a lateral size of about 600 nm, we can exclude thermal fluctuations as the primary factor triggering their motion. The second set of simulations aimed at demonstrating that, conversely, the motion of the flakes can be activated by a pulse

delivered by the tip. We represent this process by pulling the tip of a given area of the flake up to a given height, with consequent deformation of the flake. More specifically, a flake with a lateral size of 20 nm was pulled away to a distance of 3 Å from the substrate (see Fig. 4, top panel).

After being locally released from lifting (as it happens in practice while the tip scans over a specimen), the "sliding barrier" is overcome and the flake slides over the graphene surface (Fig. 4, middle and bottom panels). In fact, when the tip is detached, the deformation energy is released and converted into translational motion, after some flexural-like oscillations propagating from the tip pulling location. The transition phase lasts for ~ 200 ps, after which the flake starts to rotate and then translate, at the initial velocity of 7 pm·ps^{-1}. The flake velocity upon motion activation is found to be 2–4 pm·ps^{-1}. The total transferred energy (ΔE) from the tip to the flake is higher than ~ 2 eV, and is subsequently distributed over the atoms of the flake, allowing it to overcome the motion activation barrier in less than a few

nanoseconds. We observe that the transferred energy ΔE depends on the deformation of the flake due to the pulling, which, being local, is basically independent on the size of the flake. Therefore, it is expected that smaller flakes are activated more easily and rapidly by the tip, while larger flakes might require longer times or stronger pulling to be activated within microscopic time scales. In fact, a more efficient momentum transfer from the tip might occur with dragging- or pushing-type interactions (only a pulling-type process is considered in the simulations).

It should be noted that, once the static friction barrier is overcome, the flake enters a different regime, where the dynamic friction comes into play. This was estimated by a set of simulations where the flakes were forced to slide horizontally (by applying a constant force per unit surface) and overdamped, so that they adiabatically followed the energy profile (see Fig. 3(d) and the ESM). In this case, the fluctuations are small, and the energy profile is substantially independent on the size. As it can be seen from Fig. 3(d), the profile follows the superperiodicity of the moiré
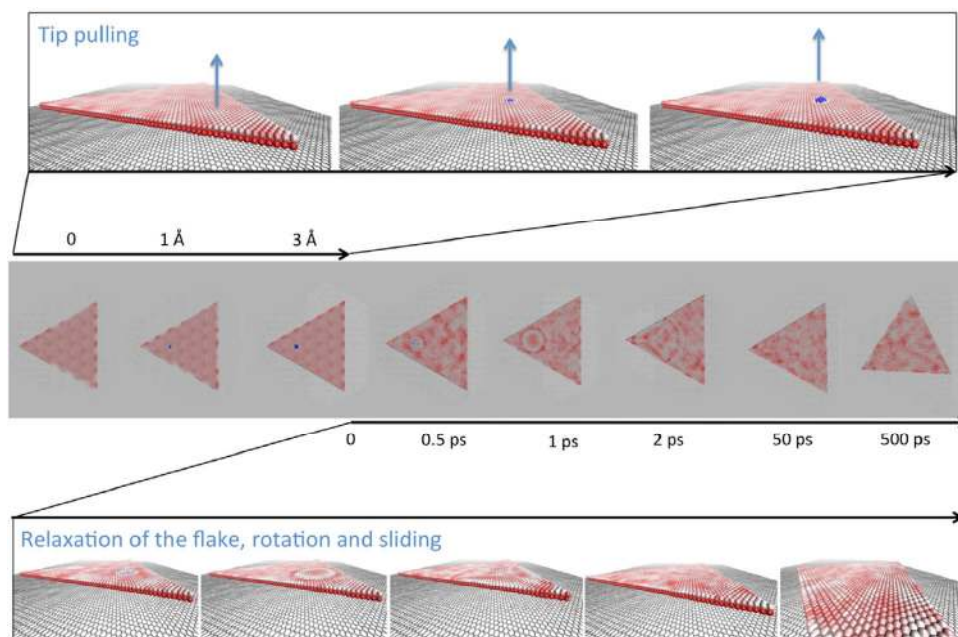

Figure 4 Simulation of pulling process of the flake with the tip up to a deformation of about 3 Å, followed by subsequent release, and free dynamics. The simulation was carried out for 1 ns at room temperature. Only selected, relevant snapshots are included; they are displayed in top view in the central strip and in perspective view in the upper and lower parts of the figure. Graphene is colored in grey, whereas the flake is colored according to its vertical displacement (with white/blue and red colors denoting protruding and intruding arrangements, respectively). The coloring pattern shows the deformation waves from the tip contact point, propagating to the flake and triggering its horizontal motion.

pattern with local fluctuations due to the atomic structure, and the barriers are of the order of 0.5–1 meV, much smaller than the motion activation barrier and $k_{B}T$. This means that, once activated, the flake motion proceeds with ultralow friction at RT, in a superlubric fashion.

However, it should be noted that in the realistic case of a surface with atomic steps, the superlubric motion is hampered by the presence of such atomic corrugations. As experimentally observed, step edges are the preferential (often temporary) locking positions for a flake. In fact, as it can be seen in the AFM videos in the ESM, in some instances the WS_2 flakes overcome atomic steps and continue their sliding motion. In order to explain this finding, it is necessary to point out that graphene grows in a carpet-like fashion on SiC [39, 40], and therefore the steps faced by the WS_2 flake are less abrupt, i.e., they are "atomically smoothened" by the presence of a continuous graphene overlayer. Hence, the step is seen by the flake as a rather sweet foot of a hill, with a local curvature that is not particularly strong (i.e., the flake does not suddenly have to climb a 7.5 Å height). From a microscopic point of view, overcoming a corrugation is favored by fluctuations, which bend the edges and vertices of the flake. The simulations show that, at RT, the root mean square fluctuations of atoms in the center of the flake are less than 1 Å, but increase up to 1–2 Å at the vertices (or 3–5 Å when the motion is triggered by the tip). Generally, dissipation occurs by releasing a certain amount of momentum at a corrugation, depending on its amplitude: The released momentum is very small in the quasi-flat case, leading to high lubricity, while it may increase for large corrugation amplitudes, up to a complete stop in particular cases.

3.3 Atomically resolved imaging of WS_2 on graphene

The reported sliding of WS_2 on graphene makes atomic resolution measurements of the heterostack extremely challenging. It should be mentioned that no STM studies have investigated the WS_2/graphene heterostructure to date, while WS_2 nanoclusters on Au(111) surfaces have been investigated [6, 41]. STM images of the more complex $Mo_{1-x}W_xS_2$ system on graphite were reported in Ref. [42]. In order to obtain

atomically resolved micrographs, it is crucial to image small-size frames entirely located within a WS_2 flake, without including flake edges. In general, we observed an increased sliding probability when the tip was positioned for an extended period in close vicinity of an edge of the flake. In the simulations, larger fluctuations were always observed at the edges than in the center of the flake; therefore, it is reasonable to expect that the tip has a stronger effect if applied laterally. Figure 5(a) shows an atomically resolved STM micrograph obtained with a sample bias of 0.1 V and a tunneling current of 0.25 nA.

A number of defective sites can be observed in the image and can be reasonably attributed to sulfur vacancies, generated either during the CVD growth process or upon exposure of the sample to the electron beam for SEM imaging [43–45].

The epitaxial alignment of the two crystals, which exhibit different lattice parameters (i.e., 3.15 Å for WS_2 and 2.46 Å for graphene [5, 46]), could result in the emergence of a moiré pattern. As a matter of fact, a number of studies investigating similar systems (i.e., MoS_2 on graphene or graphite) evidenced the presence of a moiré pattern and of modifications in the electronic band structure of the TMD [34, 35, 47]. However, no moiré pattern is observed in our case, as demonstrated in Fig. 5(a). According to the present molecular dynamics simulations, a moiré superlattice essentially emerges only at 0 K. The superpotential is disrupted by fluctuations at higher temperatures, and is no longer visible at 300 K. The absence of moiré patterns is in agreement with Ref. [5], in which no evidence of moiré superlattice features was observed in the band structure of a WS_2/graphene
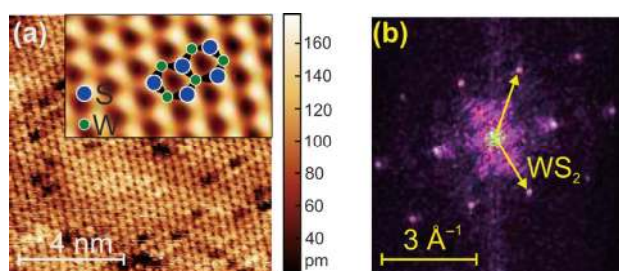

Figure 5 Atomically resolved images of WS_2 on graphene. (a) STM image (0.1 V tip voltage, 0.25 nA tunnel current) of a WS_2 flake. Inset: enlarged view of the lattice (2D FFT-filtered), with superimposed atomic positions. (b) FFT of the raw image displayed in (a).

heterostructure, further confirming the weak interaction between WS_2 and graphene. The inset in Fig. 5(a) displays a 2D fast Fourier transform (FFT)-filtered enlarged view of the image. We assigned the brightest spots to the S atoms in the top layer of the S–W–S sandwich structure, and the lower-intensity ones to the W atoms. Intuitively, this assignment would be in contradiction with the fact that the contribution of the metal atom to the density of states in WS_2 is significantly stronger than that of the S atom. However, simulated STM images for the filled states [48] indicate that geometrical effects dominate in such TMDs (the metal atoms are positioned about 1.5 Å below the S atoms). Hence, the S atoms make a larger contribution to the tunnel current, which leads to the observed triangular pattern. A FFT of the STM image was performed to visualize the hexagonal Brillouin zone of the WS_2 structure, revealing a lattice parameter of 3.2 ± 0.1 Å, as shown in Fig. 5(b). This value is in agreement with that reported for strain-free WS_2 [49], further confirming that the WS_2/graphene is a weakly interacting system.

4   Conclusions

In summary, we reported the superlubric sliding behavior of monolayer WS_2 on epitaxial graphene, triggered by a scanning probe. The WS_2/graphene heterostack examined in this study presents a predominantly 0° azimuthal alignment and an atomically sharp interface, as demonstrated by microscopic and diffraction measurements. Sliding of the WS_2 flakes is observed with a high incidence, although it appears to be stochastically triggered. Molecular dynamics simulations indicate that the motion is triggered by the tip-sample interaction and confirm that WS_2 flakes slide on graphene with ultralow friction. Thermal activation is found to be a motion-triggering factor only for flakes with lateral size one order of magnitude lower than those examined in the experiments. Since contaminants such as hydrogen can hinder superlubricity, the observation of superlubric sliding of WS_2 flakes on graphene is a further indication of the cleanliness of the CVD growth of WS_2 [50]. AFM analyses reveal that superlubric sliding is obtained also in ambient conditions. These findings highlight the promising potential of the WS_2/graphene heterostacks for novel applications as nanomotors, nanoelectromechanical systems (NEMS), and advanced optoelectronic multifunctional devices.

References

[1] Lotsch, B. V. Vertical 2D heterostructures. *Annu. Rev. Mater. Res.* **2015**, *45*, 85–109.

[2] Novoselov, K. S.; Mishchenko, A.; Carvalho, A.; Castro Neto, A. H. 2D materials and van der Waals heterostructures. *Science* **2016**, *353*, aac9439.

[3] Liu, L. T.; Kumar, S. B.; Ouyang, Y. J.; Guo, J. Performance limits of monolayer transition metal dichalcogenide transistors. *IEEE Trans. Electron Devices* **2011**, *58*, 3042–3047.

[4] Cheng, L.; Huang, W. J.; Gong, Q. F.; Liu, C. H.; Liu, Z.; Li, Y. G.; Dai, H. J. Ultrathin WS_2 nanoflakes as a high-performance electrocatalyst for the hydrogen evolution reaction. *Angew. Chem., Int. Ed.* **2014**, *53*, 7860–7863.

[5] Forti, S.; Rossi, A.; Büch, H.; Cavallucci, T.; Bisio, F.; Sala, A.; Menteş, T. O.; Locatelli, A.; Magnozzi, M.; Canepa, M. et al. Electronic properties of single-layer tungsten disulfide

on epitaxial graphene on silicon carbide. *Nanoscale* **2017**, *9*, 16412–16419.

[6] Dendzik, M.; Michiardi, M.; Sanders, C.; Bianchi, M.; Miwa, J. A.; Grønborg, S. S.; Lauritsen, J. V.; Bruix, A.; Hammer, B.; Hofmann, P. Growth and electronic structure of epitaxial single-layer WS_2 on Au(111). *Phys. Rev. B* **2015**, *92*, 245442.

[7] Georgiou, T.; Jalil, R.; Belle, B. D.; Britnell, L.; Gorbachev, R. V.; Morozov, S. V.; Kim, Y. J.; Gholinia, A.; Haigh, S. J.; Makarovsky, O. et al. Vertical field-effect transistor based on graphene-WS_2 heterostructures for flexible and transparent electronics. *Nat. Nanotechnol.* **2013**, *8*, 100–103.

[8] Mehew, J. D.; Unal, S.; Torres Alonso, E.; Jones, G. F.; Fadhil Ramadhan, S.; Craciun, M. F.; Russo, S. Fast and highly sensitive ionic-polymer-gated WS_2-graphene photodetectors. *Adv. Mater.* **2017**, *29*, 1700222.

[9] Rossi, A.; Spirito, D.; Bianco, F.; Forti, S.; Fabbri, F.; Büch, H.; Tredicucci, A.; Krahne, R.; Coletti, C. Patterned tungsten disulfide/graphene heterostructures for efficient multifunctional optoelectronic devices. *Nanoscale* **2018**, *10*, 4332–4338.

[10] Zheng, Q. S.; Jiang, B.; Liu, S. P.; Weng, Y. X.; Lu, L.; Xue, Q. K.; Zhu, J.; Jiang, Q.; Wang, S.; Peng, L. M. Self-retracting motion of graphite microflakes. *Phys. Rev. Lett.* **2008**, *100*, 067205.

[11] Liu, Z.; Yang, J. R.; Grey, F.; Liu, J. Z.; Liu, Y. L.; Wang, Y. B.; Yang, Y. L.; Cheng, Y.; Zheng, Q. S. Observation of microscale superlubricity in graphite. *Phys. Rev. Lett.* **2012**, *108*, 205503.

[12] Martin, J. M.; Donnet, C.; Le Mogne, T.; Epicier, T. Superlubricity of molybdenum disulphide. *Phys. Rev. B* **1993**, *48*, 10583–10586.

[13] Oviedo, J. P.; KC, S.; Lu, N.; Wang, J. G.; Cho, K.; Wallace, R. M.; Kim, M. J. *In situ* TEM characterization of shear-stress-induced interlayer sliding in the cross section view of molybdenum disulfide. *ACS Nano* **2015**, *9*, 1543–1551.

[14] Hirano, M.; Shinjo, K. Atomistic locking and friction. *Phys. Rev. B* **1990**, *41*, 11837–11851.

[15] Hirano, M.; Shinjo, K. Superlubricity and frictional anisotropy. *Wear* **1993**, *168*, 121–125.

[16] Hirano, M.; Shinjo, K.; Kaneko, R.; Murata, Y. Observation of superlubricity by scanning tunneling microscopy. *Phys. Rev. Lett.* **1997**, *78*, 1448–1451.

[17] Hod, O. The registry index: A quantitative measure of materials' interfacial commensurability. *ChemPhysChem* **2013**, *14*, 2376–2391.

[18] Kontorova, T. A.; Frenkel, J. On the theory of plastic deformation and twinning. II. *Zh. Eksp. Teor. Fiz.* **1938**, *8*, 1340–1348.

[19] Guerra, R.; van Wijk, M.; Vanossi, A.; Fasolino, A.; Tosatti, E. Graphene on h-BN: To align or not to align? *Nanoscale* **2017**, *9*, 8799–8804.

[20] Dienwiebel, M.; Verhoeven, G. S.; Pradeep, N.; Frenken, J. W. M.; Heimberg, J. A.; Zandbergen, H. W. Superlubricity of graphite. *Phys. Rev. Lett.* **2004**, *92*, 126101.

[21] Feng, X. F.; Kwon, S.; Park, J. Y.; Salmeron, M. Superlubric sliding of graphene nanoflakes on graphene. *ACS Nano* **2013**, *7*, 1718–1724.

[22] Li, H.; Wang, J. H.; Gao, S.; Chen, Q.; Peng, L. M.; Liu, K. H.; Wei, X. L. Superlubricity between MoS_2 monolayers. *Adv. Mater.* **2017**, *29*, 1701474.

[23] Liu, S.-W.; Wang, H.-P.; Xu, Q.; Ma, T.-B.; Yu, G.; Zhang, C. H.; Geng, D. C.; Yu, Z. W.; Zhang, S. G.; Wang, W. Z. et al. Robust microscale superlubricity under high contact pressure enabled by graphene-coated microsphere. *Nat. Commun.* **2017**, *8*, 14029.

[24] Wang, D. M.; Chen, G. R.; Li, C. K.; Cheng, M.; Yang, W.; Wu, S.; Xie, G. B.; Zhang, J.; Zhao, J.; Lu, X. B. et al. Thermally induced graphene rotation on hexagonal boron nitride. *Phys. Rev. Lett.* **2016**, *116*, 126101.

[25] Wang, L. F.; Zhou, X.; Ma, T. B.; Liu, D. M.; Gao, L.; Li, X.; Zhang, J.; Hu, Y. Z.; Wang, H.; Dai, Y. D. et al. Superlubricity of a graphene/MoS_2 heterostructure: A combined experimental and DFT study. *Nanoscale* **2017**, *9*, 10846–10853.

[26] Leven, I.; Krepel, D.; Shemesh, O.; Hod, O. Robust superlubricity in graphene/h-BN heterojunctions. *J. Phys. Chem. Lett.* **2013**, *4*, 115–120.

[27] Rossi, A.; Büch, H.; Di Rienzo, C.; Miseikis, V.; Convertino, D.; Al-Temimy, A.; Voliani, V.; Gemmi, M.; Piazza, V.; Coletti, C. Scalable synthesis of WS_2 on graphene and h-BN: An all-2D platform for light-matter transduction. *2D Mater.* **2016**, *3*, 31013.

[28] Goler, S.; Coletti, C.; Piazza, V.; Pingue, P.; Colangelo, F.; Pellegrini, V.; Emtsev, K. V.; Forti, S.; Starke, U.; Beltram, F. et al. Revealing the atomic structure of the buffer layer between SiC(0001) and epitaxial graphene. *Carbon* **2013**, *51*, 249–254.

[29] Nečas, D.; Klapetek, P. Gwyddion: An open-source software for SPM data analysis. *Cent. Eur. J. Phys.* **2012**, *10*, 181–188.

[30] Smith, W.; Forester, T. R. DL_POLY_2.0: A general-purpose parallel molecular dynamics simulation package. *J. Mol. Graph.* **1996**, *14*, 136–141.

[31] Miwa, J. A.; Dendzik, M.; Grønborg, S. S.; Bianchi, M.; Lauritsen, J. V.; Hofmann, P.; Ulstrup, S. Van der Waals epitaxy of two-dimensional MoS_2–graphene heterostructures in ultrahigh vacuum. *ACS Nano* **2015**, *9*, 6502–6510.

[32] Liu, X. L.; Balla, I.; Bergeron, H.; Campbell, G. P.; Bedzyk,

M. J.; Hersam, M. C. Rotationally commensurate growth of MoS$_2$ on epitaxial graphene. *ACS Nano* **2016**, *10*, 1067–1075.

[33] Zhang, C. D.; Johnson, A.; Hsu, C. L.; Li, L. J.; Shih, C. K. Direct imaging of band profile in single layer MoS$_2$ on graphite: Quasiparticle energy gap, metallic edge states, and edge band bending. *Nano Lett.* **2014**, *14*, 2443–2447.

[34] Huang, Y. L.; Chen, Y. F.; Zhang, W. J.; Quek, S. Y.; Chen, C. H.; Li, L. J.; Hsu, W. T.; Chang, W. H.; Zheng, Y. J.; Chen, W. et al. Bandgap tunability at single-layer molybdenum disulphide grain boundaries. *Nat. Commun.* **2015**, *6*, 6298.

[35] Pierucci, D.; Henck, H.; Avila, J.; Balan, A.; Naylor, C. H.; Patriarche, G.; Dappe, Y. J.; Silly, M. G.; Sirotti, F.; Johnson, A. T. C. et al. Band alignment and minigaps in monolayer MoS$_2$-graphene van der Waals heterostructures. *Nano Lett.* **2016**, *7*, 4054–4061.

[36] Xu, P.; Yang, Y. R.; Qi, D.; Barber, S. D.; Schoelz, J. K.; Ackerman, M. L.; Bellaiche, L.; Thibado, P. M. Electronic transition from graphite to graphene via controlled movement of the top layer with scanning tunneling microscopy. *Phys. Rev. B* **2012**, *86*, 085428.

[37] Xu, P.; Ackerman, M. L.; Barber, S. D.; Schoelz, J. K.; Qi, D. J.; Thibado, P. M.; Wheeler, V. D.; Nyakiti, L. O.; Myers-Ward, R. L.; Eddy, C. R., Jr. et al. Graphene manipulation on 4H-SiC (0001) using scanning tunneling microscopy. *Jpn. J. Appl. Phys.* **2013**, *52*, 035104.

[38] Kobayashi, Y.; Taniguchi, T.; Watanabe, K.; Maniwa, Y.; Miyata, Y. Slidable atomic layers in van der Waals heterostructures. *Appl. Phys. Express* **2017**, *10*, 045201.

[39] de Heer, W. A.; Berger, C.; Wu, X. S.; First, P. N.; Conrad, E. H.; Li, X. B.; Li, T. B.; Sprinkle, M.; Hass, J.; Sadowski, M. L. et al. Epitaxial graphene. *Solid State Commun.* **2007**, *143*, 92–100.

[40] Lauffer, P.; Emtsev, K. V.; Graupner, R.; Seyller, T.; Ley, L.; Reshanov, S. A.; Weber, H. B. Atomic and electronic structure of few-layer graphene on SiC(0001) studied with scanning tunneling microscopy and spectroscopy. *Phys. Rev. B* **2008**, *77*, 155426.

[41] Perea-López, N.; Lin, Z.; Pradhan, N. R.; Iñiguez-Rábago, A.; Laura Elías, A.; McCreary, A.; Lou, J.; Ajayan, P. M.; Terrones, H.; Balicas, L. et al. CVD-grown monolayered MoS$_2$ as an effective photosensor operating at low-voltage. *2D Mater.* **2014**, *1*, 011004.

[42] Yoshida, S.; Kobayashi, Y.; Sakurada, R.; Mori, S.; Miyata, Y.; Mogi, H.; Koyama, T.; Takeuchi, O.; Shigekawa, H. Microscopic basis for the band engineering of Mo$_{1-x}$W$_x$S$_2$-based heterojunction. *Sci. Rep.* **2015**, *5*, 14808.

[43] Lin, Z.; Carvalho, B. R.; Kahn, E.; Lv, R. T.; Rao, R.; Terrones, H.; Pimenta, M. A.; Terrones, M. Defect engineering of two-dimensional transition metal dichalcogenides. *2D Mater.* **2016**, *3*, 022002.

[44] Parkin, W. M.; Balan, A.; Liang, L. B.; Das, P. M.; Lamparski, M.; Naylor, C. H.; Rodríguez-Manzo, J. A.; Johnson, A. T. C.; Meunier, V.; Drndić, M. Raman shifts in electron-irradiated monolayer MoS$_2$. *ACS Nano* **2016**, *10*, 4134–4142.

[45] Fabbri, F.; Rotunno, E.; Cinquanta, E.; Campi, D.; Bonnini, E.; Kaplan, D.; Lazzarini, L.; Bernasconi, M.; Ferrari, C.; Longo, M. et al. Novel near-infrared emission from crystal defects in MoS$_2$ multilayer flakes. *Nat. Commun.* **2016**, *7*, 13044.

[46] Kormányos, A.; Burkard, G.; Gmitra, M.; Fabian, J.; Zólyomi, V.; Drummond, N. D.; Fal'ko, V. Corrigendum: k.p theory for two-dimensional transition metal dichalcogenide semi-conductors (2015 2D Mater. 2 022001). *2D Mater.* **2015**, *2*, 049501.

[47] Liu, X. L.; Balla, I.; Bergeron, H.; Hersam, M. C. Point defects and grain boundaries in rotationally commensurate MoS$_2$ on epitaxial graphene. *J. Phys. Chem. C* **2016**, *120*, 20798–20805.

[48] González, C.; Biel, B.; Dappe, Y. J. Theoretical characterisation of point defects on a MoS$_2$ monolayer by scanning tunnelling microscopy. *Nanotechnology* **2016**, *27*, 105702.

[49] Füchtbauer, H. G.; Tuxen, A. K.; Moses, P. G.; Topsøe, H.; Besenbacher, F.; Lauritsen, J. V. Morphology and atomic-scale structure of single-layer WS$_2$ nanoclusters. *Phys. Chem. Chem. Phys.* **2013**, *15*, 15971–15980.

[50] Dong, Y. L.; Wu, X. W.; Martini, A. Atomic roughness enhanced friction on hydrogenated graphene. *Nanotechnology* **2013**, *24*, 375701.